Journal of Materials Chemistry A

Accepted Manuscript

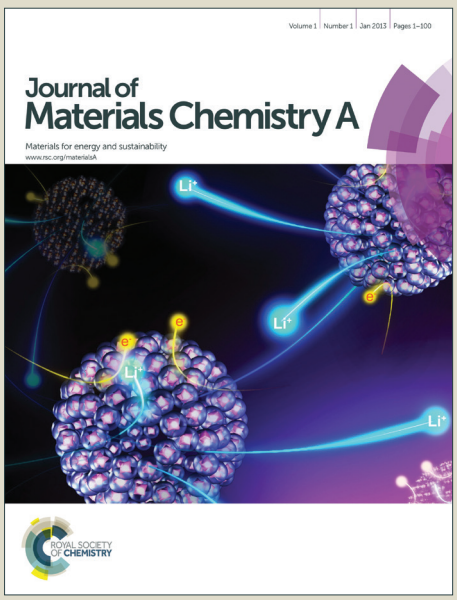

ROYAL SOCIETY OF CHEMISTRY

www.rsc.org/materialsA

Journal Name

ARTICLE

Facile Ion-exchange Synthesis of Silver Films as Flexible Current Collectors for Micro-Supercapacitors

Received 00th January 20xx,

Accepted 00th January 20xx

DOI: 10.1039/x0xx00000x

www.rsc.org/

Yizhen Yu,[a] Jian Zhang,*[a] Xing Wu,[a] and Ziqiang Zhu[b]

A universal and facile methodology for high flexible supercapacitors with silver current collectors fabricated by ion-exchange surface metallization has been developed. The supercapacitors show high conductivity of 1.68×10^5 S cm^{-1}, and high mechanical strength with more than 16 000 bending cycles. With multiple walled carbon nanotube as the electrode material, the micro supercapacitors (MSCs) with symmetric interdigitated electrodes were fabricated at room temperature. MSCs allow for operations at high rate up to more than 200 V s^{-1}, two orders of magnitude higher than that of conventional supercapacitors. With robust Ag current collectors, high cycling properties had been obtained which are verified by CV testing. MSCs can bear more than 15 000 cycling testing and the content can maintain more than 97%. The developed polymer metallization technique is potential to construct the whole electronic system on one chip.

Introduction

Nowadays, the energy storage devices with large flexibility, high miniaturization and independent operation system are strongly desired for the rapidly developed wearable electronic technologies. For large-scale electronic systems, the oversized battery is always problematic. Instead of using macro-primary batteries, a large research effort had been directed towards developing microscale ambient energy harvesters and complementary micro-energy storage devices. To fulfill specific wearable and portable applications, the ultimate target is that the whole flexible system, containing working devices, energy storage and energy harvester, shall be integrated on one chip.[1] The combination of energy storage and energy harvester incorporates the ability to convert ambient energy (e.g., solar, vibration, thermal energy, etc.) into useful electrical energy, which is then stored in an energy reservoir until needed by the microdevices. Polymeric substrates, with the reduced weight and the enhanced flexibility, are preferred to fulfill this demand.

Currently, the complexity in integration is an obstacle which impedes the application of low cost flexible electronic device. For example, the traditional polymer metallization such as physical vapor deposition (PVD) and chemical vapor deposition (CVD) normally require expensive facilities, complex processes or high temperatures.[2-4] One primary solution is to develop a universal fabrication technique which can process in open air and room temperature. Surface metallization via ion exchange (SMIE), *in-situ* growth of thin films from chemical solution, can perfectly meet this requirement.[5-8]

SMIE is a technique which can be used to grow conductive metal films on the polyimide substrate. Previously, for the first time, our group has reported a flexible humidity sensor by this technique.[9] Since the energy storage plays an important role in functional flexible systems[10, 11] and micro-supercapacitors (MSCs) are the workhorse energy storage device drawn lots of attentions,[1, 12, 13] in this paper, we studied the potential application of SMIE in MSCs construction. In current MSCs, complicated IC processes like sputtering and photolithography are always inducing tedious fabrication processes and high cost.[14-20] To achieve high performance and rate capability, various MSC constituents including the metal current collectors (MCCs), the electrode active materials, and the electrolyte need to be optimized.[16, 21] MCCs are typically electrochemically inactive with the electrolyte and are usually electrically conductive materials applied as thin films, meshes or coatings to the device electrodes. MCCs are often used to guide and quickly direct charges to the active materials and are critical to time constant which measures the charge/discharge capability of MSCs. The criteria to evaluate MCCs include the cost, the electrical conductivity, the stability, the processing compatibility, as well as the stability characterized with cycling numbers, working temperature, and the electrochemical environment.[22, 23] For the flexible devices, the balance between high electrical conductivity and large mechanical flexibility will be a big challenge for MCCs.

Here, a cleanroom-free, simple and low-cost fabrication approach utilizing a SMIE Ag MCCs for flexible MSCs was developed. The novel Ag MCCs enable both ultrahigh

[a] *Shanghai Key Laboratory of Multidimensional Information and Processing, the Key laboratory of Poling Materials and Devices, DOE, East China Normal University, 500 Dongchuan Road, 200241Shanghai, China, Email: jzhang@ee.ecnu.edu.cn*

[b] *Department of Physical, Shanghai Normal University, 100 Guilin Road, 200062, Shanghai, China*

† Footnotes relating to the title and/or authors should appear here. Electronic Supplementary Information (ESI) available: [details of any supplementary information available should be included here]. See DOI: 10.1039/x0xx00000x

mechanical strength and high electrical conductivity simultaneously. With CNTs as the active material, the MSCs can work even at a scan rate of 200 V s^{-1} with the minimum time constant of 11.3 ms. Moreover, the MSCs is able to bear 16 000 bending cycles without performance degradation. This result is superior to previously flexible MSCs.[24] This technique offers great advantages including simple processing, low cost and batch fabrication, and is readily scalable and applied to mature industrial roll-to-roll process.

Experimental

Materials and reagents

Commercial available ~50 μm pyromellitic dianhydride-oxydianiline (PMDA-ODA) polyimide films (PI) were purchased from Qian Feng Insulating Material Company (Shanghai, China). KOH, $NH_3 \cdot H_2O$, $AgNO_3$ (99.8%) purchased from Aladdin Industrial Corporation (Shanghai, China) were used without further purification. MWNT and the dispersion were supplied by BoYu GaoKe, China. The photosensitive dry films with thickness of 50 μm, covered with blue protective layer, were produced by Xide Electronic, China.

Preparation of Interdigital Electrode

After carefully cleaned in acetone, ethanol, and DI water, the flexible PI substrate bonded to the glass substrate were immersed in 4 M KOH aqueous solution for 90 min at room temperature and washed with sufficient amount of ethanol and DI water subsequently. The photosensitive dry films were stuck tightly to the treated PI. The prepared films were exposed in open-air for 1 min with patterned IDE films used as mask. Then the exposed PI was developed with 0.1 M $NaHCO_3$ to form interdigital electrodes (IDEs) patterns. Next, mask-protected PI films were soaking in 0.02 M $Ag(NH_3)_2^+$ solution for 10 min. The protected PI films were further dipped into in 0.02 M H_2O_2 for 1-2 min until the shiny Ag films were obtained on the exposed PI regions. So far, Ag films were selectively grown onto PI substrate and the Ag IDEs on PI were prepared.

Preparation of Ag/MWNT IDEs

For the active material preparation, 90 wt% MWNT and 10 wt% MWNT dispersion agents were mixed in DI water and sonicated for 1 hour. The PI films with Ag IDEs were dipped into the MWNT solution and dried. By this procedure, the active MWNT material was selectively deposited onto Ag IDEs. Then, the masking photosensitive films were removed by acetone. At last, Ag/MWNT IDEs were achieved.

Fabrication of SMIE-MSCs

For solid electrolyte preparation, 5 ml H_3PO_4, 50 ml DI water and 5g PVA powder were mixed. The solution was stirred at 85 °C until the solution became a clear gel. Next, 0.01 ml gel solution was dropped carefully on Ag/MWNT IDEs. After vaporizing the excess water, an all-solid-state SMIE-MSC was obtained.

SMIE-MSCs Characterization

The microstructures of SMIE-MSCs were investigated by means of scanning electron microscopy (SEM, Hitachi S4800), atomic force microscope (AFM, Nano Navi SII E Sweep) and optical microscopy (Caikon DMM-2200). The chemical composition was characterized by Fourier transform infrared spectroscopy (FTIR, Nicolet 6700), X-ray diffraction (XRD, Rigaku D/Max2500VB2+/PC), and X-ray photoelectron spectroscopy (XPS, AXIS UltraDLD). Electrical measurements were carried out on Hall effect measurement system (RH2035). The electrochemical properties of MSCs were investigated with cyclic voltammetry (CV), chronopotentiometry (CP) and electrochemical impedance spectroscopy (EIS) measurements, using CHI660D electrochemical workstation. The electrochemical impedance spectroscopy (EIS) was taken in the frequency range from 100 kHz to 0.01 Hz with potential amplitude of 5 mV. Adhesion of thin metalized films to their substrates was first characterized using a simple adhesive tape peel test (cross-cut tape test of type-ASTM D 3359 3M, Scotch, magic tape 810). The flexing or bending test was undergone on the mechanical stirring machine (Shanghai Lushuo JB50-D, China).

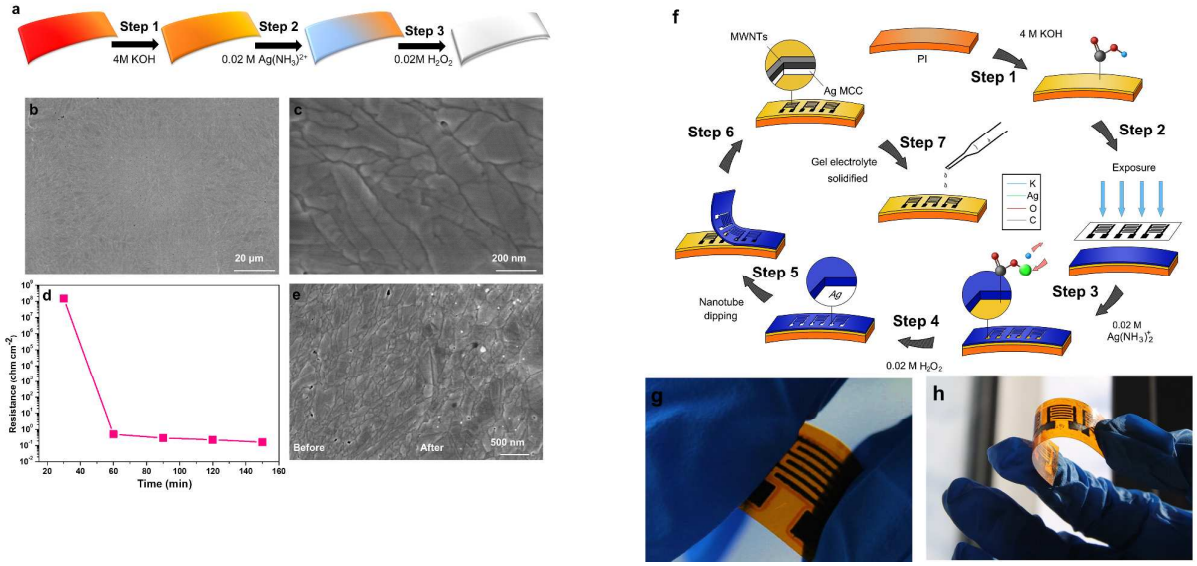

Fig. 1 Fabrication and characterization of SMIE-Ag film and MSCs. (a) The fabrication process of SMIE-Ag film. (b-c) SEM images of surface on SMIE-Ag film. (d) Time KOH immersion versus square resistance. (e) Comparison of SMIE-Ag surface before and after peeling with adhesive tape. (f) Flow chart for MSCs fabrication on PI substrate with SMIE technique. (g-h) Photographs of as-received flexible MSCs.

Journal Name

ARTICLE

Results and discussion

Fig. 1a illustrates the main processes of SMIE technique. To grow metal films on polyimide by SMIE, the procedure comprises the PI hydrolysis in alkali solution resulting in the cleavage of imide rings and the formation of carboxylic acid groups (Step 1 in Fig. 1a), the metal ions loading through ion exchange between the carboxyl groups and the metal salt aqueous solution (Step 2 in Fig. 1a), and the final reduction reaction to generate the metal films (Step 3 in Fig. 1a).

PI surface was chemically modified into potassium-polycarboxylate salt[7, 8], and K^+ ions were embedded in PI, as indicated by the PI color changing from orange to yellow (Step 2 in Fig. 1a). The PI films were then soaked in 0.02 M $Ag(NH_3)_2^+$ solution for 10 min. The embedded K^+ ions in film were replaced by Ag^+ ions through ion exchange. The obtained PI films were further dipped into 0.02 M H_2O_2 for 1-2 min until the shiny Ag layers were obtained. So far, Ag films were grown onto PI substrate. The modification of PI surface was identified by FTIR (Fig. S1†).

Through XRD analysis, four diffraction peaks, corresponding to [111], [200], [220], [311], respectively, can be found between 30° and 80° (Fig. S2†), which is in agreement with the JCPDS No. 4-783. The result indicates that Ag films are constructed by face-centered cubic Ag crystalline particles. XPS analysis also shows the strong Ag 3d peak. And the Ag mass content is up to 88% (Fig. S3†).

Fig. 1b, c are the scanning electron microscopy (SEM) pictures of Ag films with different magnified factors. The whole Ag film surface is flat and the film is composed of tightly arranged Ag nanoclusters. The obvious continuity of Ag film indicates that this film is well conductive.

From Fig. 1d, the conductivity of Ag thin films can be adjusted by the soaking time in 4 M KOH solution. Longer soaking time leads to lower resistance. When the soaking time reaches 60 min, the Ag film becomes highly conductive with area resistance of 0.165 to 0.5 Ω cm^{-2}. Since the thicker Ag films will lead to less flexibility, the optimized soaking time is 90 min.

Fig. 1e are SEM pictures showing the Ag film surfaces before and after adhesive tape peeling testing, in which the white spots in the right picture are the residuals from the adhesive tape. From the picture, no obvious changes could be found, implying the peeling damage is negligible and the adhesion strength between silver layers and polyimide substrate is superior. This strong adhesion is attributed to the fact that unlike the conventional PVD coating process, the Ag films are grown from the internal of modified PI substrate. [7, 8]

Fig. 1f illustrates the whole fabrication process of SMIE-MSCs. In Fig. 1f, Step 1-4 and 5, 6 are the steps of Ag MCCs fabrication and Ag/MWNT IDEs preparation, respectively.

The PI substrates are first treated in KOH as previously mentioned (Step 1 in Fig. 1f). The photosensitive dry films are stuck tightly to the treated PI. The PET transparency films with inkjet-printed IDEs patterns are used as mask and the lithography is processed without clean room (Step 2 in Fig. 1f). The interdigital patterns are formed on PI after developed in $NaHCO_3$ (0.1 M) solution. Then, the mask-protected PI films are soaked in 0.02 M $Ag(NH_3)_2^+$ solution for 10 min (Step 3 in Fig. 1f). The doped K^+ ions (the blue ball in Fig. 1f) in films were replaced by Ag^+ ions (the green ball in Fig. 1f). The protected PI films are further dipped in $Ag(NH_3)_2^+$ to in 0.02 M H_2O_2 for 1-2min until the shiny Ag layers are obtained on the exposed PI regions (Step 4 in Fig. 1f). So far, Ag IDEs are selectively grown onto PI substrate.

To achieve Ag/MWNT IDEs, MWNT dispersion is dip-coated onto the as-prepared Ag MCCs and the masking layers are removed by acetone (Step 5 in Fig. 1f). By this procedure, the active MWNT material is selectively deposited onto Ag IDEs (Step 6 in Fig. 1f). No complex processes like pattern transfer and annealing are needed. [20, 24]

The H_2SO_4/polyvinyl alcohol (H_2SO_4/PVA) gel is used as electrolyte.[19, 20] 0.01 ml gel solution is dropped casting on Ag/MWNT IDEs carefully. After the excessive water is vaporized, an all-solid-state SMIE-MSC is obtained. The gel electrolyte also acts as simplified packaging materials to protect MSC from damage.

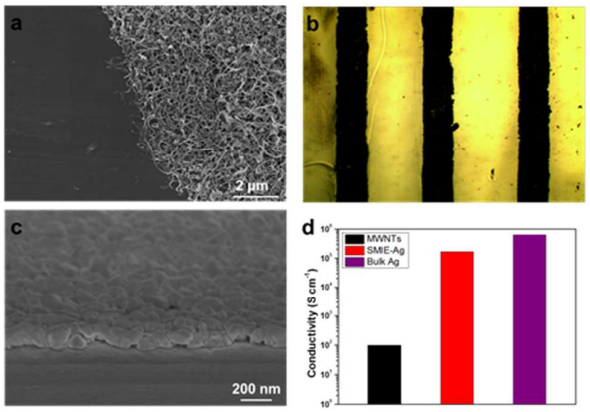

Fig. 2 Characterization of Ag-MCCs and MSCs. (a) A SEM image of the boundary between PI substrate and MWNT electrode. (b) An optical microscope image of MWNT IDEs. (c) A SEM image of the Ag MCC. (d) A comparison of electrical conductivities among MWNTs, SMIE-Ag and bulk Ag.

Fig. 1g, h show the photographs of as-received flexible MSCs and MSCs arrays. The length and width of each finger is 8mm,

and 500 μm, respectively, and the interspace is 500 μm. Therefore, the calculated fingerprint area of IDE is about 0.44 cm^2. As shown in Fig. 2a, the profile between MWNTs electrodes and PI substrates is clear and well defined. The as-received Ag/MWNT IDEs' thickness is ~2 μm (Fig. S4†), which can be obtained from AFM. With our method, the minimum MWNT IDEs' width can be ~100 μm (Fig. 2b). Fig. 2c is the SEM picture of Ag MCCs. The thickness of Ag MCCs was around

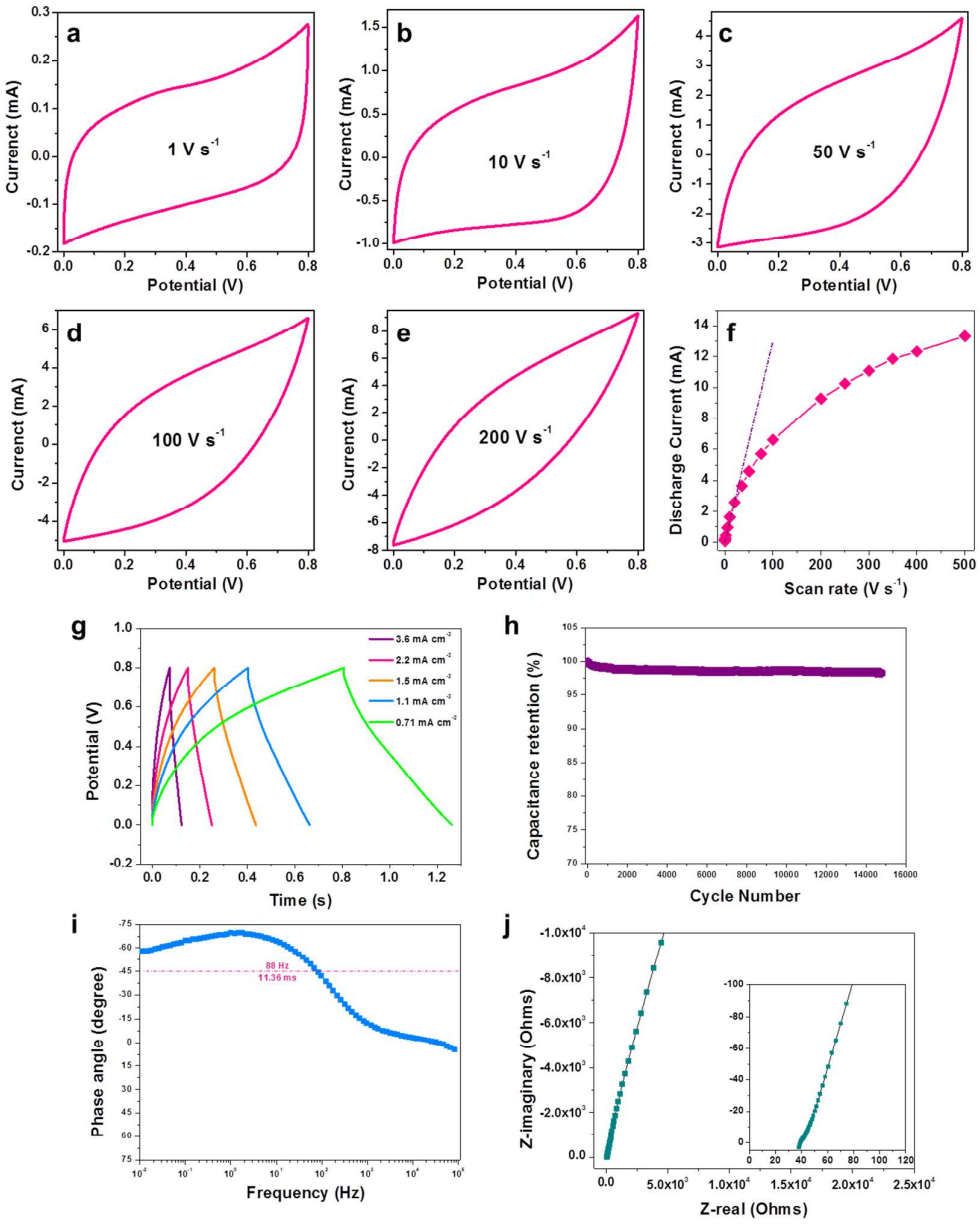

Fig. 3 (a-f) CV curves for MSCs at 1-200 V s^{-1}. (f) A plot of the discharge current as a function of the scan rate. (g) Galvanostatic charge/discharge curvesat 0.71-3.6 mA cm^{-2}. (h) Cycling stability at 20 V s^{-1}. (i) Impedance phase angle versus frequency with calculated time constant. (J) Complex plane plot of the impedance of a SMIE-MSC with a magnification of the high-frequency region is provided in the inset.

200 nm. Fig. 2d demonstrates that the measured conductivity of Ag film is 1.68×10^5 S cm^{-1}, which is much higher than the coated WMNTs, 100 S cm^{-1}, and close to the bulk Ag, 6.3×10^5 S cm^{-1}. It is found that for those MCC-free MSCs, the performances of devices were confined by the low conductivity of active material electrodes, which act as the electrode simultaneously.[25-27]

CV has been used to investigate the MSCs. In principle, the higher level of CV scanning rate, the higher instantaneous power MSC can undergo. Fig. 3a-e show the CV results of the scan rate of 1, 10, 50, 100 and 200 V s^{-1}, with the potential window of 0-0.8 V, respectively. Up to 50 V s^{-1}, nearly rectangular CV shapes could be observed, indicating the typical double-layer capacitive behavior was dominant and the SMIE-MSCs showed outstanding electrochemical performance. Noticeably, even with charged and discharged rate rapidly up to 200 V s^{-1}, MSCs still maintained fine capacitance behavior. This scan rate is more than two orders of magnitude higher

than those of conventional MSCs, and even better than many MSCs based on fine lithography and PVD processes.[26-30] The fast charge/discharge rate could be attributed to the highly conductive Ag MCCs. The respective specific area capacitances in the scan rate of 1 and 200 V s^{-1} are 562 and 108 μF cm^{-2}, respectively (Fig. S5†).

Fig. 3f clearly shows the dependency of the discharge current versus the scan rate. Linear dependence of the discharge current is found up to 35 V s^{-1}, demonstrating the high power ability of MSCs.[19]

These conclusions are also confirmed by galvanostatic charge/discharge testing. Galvanostatic charge/discharge testing was performed from 0.71 up to 3.6 mA cm^{-2} (Fig. 3g). When the current density is 0.71 mA cm^{-2}, the voltage dropped at the beginning of each discharge curve, known as the iR drop, is negligible, indicating a very low internal series resistance for MSCs. To some degree, this is due to the introduction of high performance Ag MCCs. As the currents density increased up to > 1 mA cm^{-2}, the iR drop begins to rise but is still acceptable. This tolerable charge/discharge current is remarkably bigger than many published results.[23, 26-28, 31]

The MSCs' performance cycled up to 15 000 times at scan rate of 20 V s^{-1} is shown in Fig. 3h. After 15 000 cycling testing, the flexible MSCs still could maintain over ~97% of its original capacitance. The lifetime CV cycling curve shows that the MSCs thus developed exhibit robust cycling stability. The long lifespan also demonstrates the chemistry stability of Ag MCCs. This property is competitive to other high cost MSCs, and even better than some MSCs based on clean room techniques.[19, 30, 32]

The time constant τ can be obtained from EIS data analysis, which can demonstrate the cycling ability. In principle, both the electrode's interspace and the MCCs' resistance affect τ. To achieve low τ value, the MCCs' resistance must be sufficient low.[16] As shown in Fig. 3i, the frequency for SMIE-MSCs at a phase angle of -45° is about 88 Hz. The calculated τ is 11.3 ms ($\tau = 1/f_0$). This result is better than these MCC-free devices like laser-scribed graphene MSCs with 19 ms and onion-like carbon with 23 ms.[18, 22] So far laser patterning technology is regarded as a potential solution to produce microdevice.[22, 25, 27, 33-35] For example, W Gao reported direct laser writing MSCs.[25] El-Kady introduced LSG-MSCs.[22, 34] In these studies, since no specially designed MCCs were employed, the conductivity of active material electrode, acting as the current collectors simultaneously, was quite low, only 2.8×10^{-3} S cm^{-1} and 2.35×10^{3} S m^{-1}, respectively, which led to the lower performance.

Compared to other similar MSCs with CNT as active materials, τ is also obviously reduced.[17] Moreover, considering the large interspace, of ~ 500 μm, and the simple process employed in this study, τ can be further decreased if the narrower interelectrode space is employed and the processes are optimized.

Fig. 3j shows the Nyquist plot measured by Electrochemical Impedance Spectroscopy (EIS). EIS plot is quite close to imaginary axis, which is the typical characteristic of the pronounced capacitive behavior. No semicircle in EIS plot can be found. This is due to the short ion diffusion pathway for IDE configuration. The equivalent series resistance of MSCs is ~39 Ω, which is among the level of previously reported all-solid-state MSCs.[19, 20, 36, 37]

To examine the mechanical property of SMIE-MCSs, both electrical property and mechanical property should be taken into consideration. So far for most reported MSCs, only the testing in different bending radii or the cycling at fixed bending states are performed.[19, 22, 38] However, this is not enough to characterize the mechanical performance.[24] To examine the flexibility of our MSCs, two testing schemes, are designed and performed.

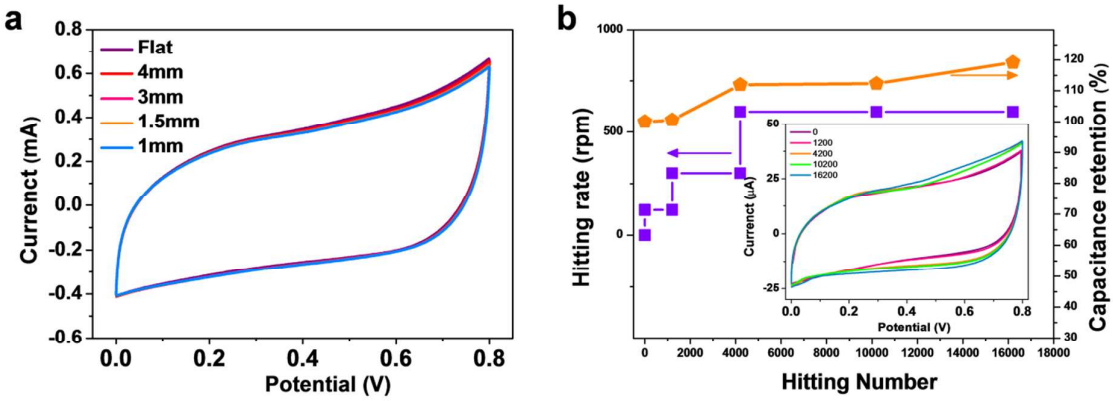

Fig. 4 Mechanical testing results of SMIE-MSCs. (a) Comparison of CV curves under different bending states. (b) Hitting rate and capacitance retention versus hitting numbers in 16000 hittings. The inset plot is comparison of CV curves under different hitting number in 16000 hittings.

In Scheme I, the mechanical bending property of MSCs is measured on a common adjustable spanner with two clamps (Fig. S6†). Under various bending states, cyclic voltammetry measurements are conducted at a fixed scan rate of 3 V s^{-1}. The C-V curves under different bending states are shown in Fig. 4a. It can be seen when the curvature radii range from 4mm to 1mm, no obvious changes of C-V curves can be found. Even under the maximum bending state with curvature r=1 mm, C-V curves still keep almost the same as the flat state. The working curvature ranges in this study was more rigorous than other

previously reported MSCs.[19, 20, 22, 23, 37] The bending measurement has demonstrated that our MSCs have highly robust stability and are likely to be applied to the flexible and wearable applications.

In Scheme II, by choosing the bending duration cycle, the wearable duration of SMIE-MSCs under physical wear and tear process is also examined. The testing is done through a mixer machine (Fig. S7†). The blade of machine could hit the free-end of MSCs every cycle and cause the bending. Upon hitting, the deflection angle is ~30°, corresponding to the original MSCs plane. The bending rates, determined by the rotation speed of machine, can be adjusted from 120 rpm to 600 rpm. Cyclic voltammetry measurements are conducted at the scan rate of 0.2 V s^{-1}, with capacitors of different numbers of flexing cycle. The test results are shown in Fig. 4b. From first 1200 cycles with the rotation speed of 120 rpm, the CV shape and the capacitance retention keep unchanged. When the hitting rate and the hitting cycle rise to 600 rpm and 16 000, respectively, the MSCs still can work normally.

Ragone plot which shows the specific power versus the specific energy of different energy storage devices has been plotted in Fig. 4. MSCs of this work, printed MSCs with N-doped rGO,[39] G/CNTCs-MSCs,[17] commercial high-energy thin-film lithium battery,[18] high power aluminum electrolytic capacitor[25] and Panasonic Li-ion battery[20] have been chosen. The power density and the energy density of SMIE-MSCs range from 0.053 to 57.8 W cm^{-3} and 0.001 to 2.5 W cm^{-3}, which are better than the G/CNTCs-MSCs fabricated on rigid substrates.

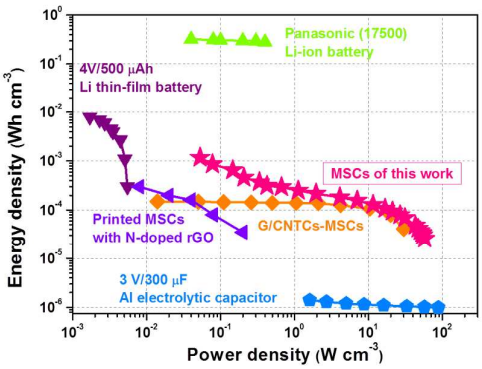

Fig. 5 Ragone plot for the developed MSCs. The comparison of energy and power densities of SMIE-MSCs with G/CNTCs-MSCs, Printed MSCs with N-doped rGO, commercially available electrolytic capacitors, lithium thin-film batteries , Panasonic Li-ion battery

The combination of photosensitive dry films and PI metallization can produce flexible SMIE-MSCs without any extra processes like annealing and transferring. This enables SMIE technique a potential solution to integrate different devices, like sensor, energy storage and harvester, on the same chip, just as shown in Fig. 5.

Metallization methods employed in traditional flexible MSCs include PVD, CVD, electrodeposition, and electroless plating, screen printing and etc, which are either labor-intensive or facilities-required. Moreover, the resulted films have very poor adhesion to the substrate, which shortens the lifespan and degrades/deteriorates the performance of flexible electronics devices. With our SMIE technique, all processes are done at room-temperature. No anionic groups, such as Cl^-, SO_4^{2-} and NO_3^-, are incorporated into the films, which is benefit to maintain the excellent electrical and mechanical properties.

The microstructures and the thickness of metal layers can be systematically controlled by initial alkali treatment and subsequent SMIE conditions (concentration, time and temperature), as well as by the final reduction procedure. The developed method is applicable not only to some other metals, such as Au, Pt, Ni, Cu, Co, Pd, and etc., but also some other active materials, such as graphene, PANI, MnO_2, NiO, and etc..[15-17, 19, 20, 37]

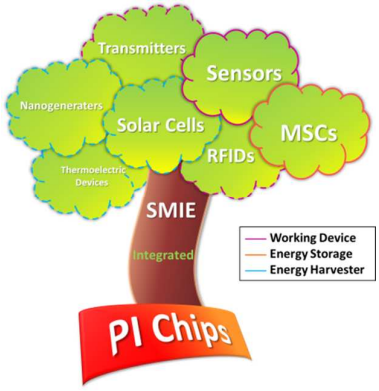

Fig. 6 Structure of SMIE technique. SMIE technique can applied various devices of different functions on PI substrates to form PI chips.

Conclusions

In summary, we have fabricated the flexible MSCs with SMIE technique. The whole fabrication process is completed in open air and does not involve any complicated clean room processes, like RF-sputtering and lithography. MSCs of this work offers high power density, high flexibility and long endurance, especially the ultra-high mechanical strength. This work provides a facile, scalable, low-cost approach to fabricate MSCs with promising application as integrated on-chip energy storage unites for flexible devices.

Acknowledgements

This work was supported by Projects of Science and Technology Commission of Shanghai Municipality (Grant No. 15JC1401800).

Notes and references

1 M. Beidaghi, and Y. Gogotsi, *Energy Environ. Sci.*, 2014, **7**, 867. Citations should appear here in the format A. Name, B. Name and C. Name, Journal Title, 2000, 35, 3523; .A. Name, B. Name and C. Name, *Journal Title*, 2000, **35**, 3523.
2 C.-Y. Lee, G.-W. Wu and W.-J. Hsieh, *Sens. Actuators, A*, 2008, **147**, 173.
3 S. Y. Xiao, L. F. Che, X. X. Li and Y. L. Wang, *Microelectron. Eng.*, 2008, **85**, 452.

4 E. Zampetti, S. Pantalei, A. Pecora, A. Valletta, L. Maiolo, A. Minotti, A. Macagnano, G. Fortunato and A. Bearzotti, *Sens. Actuators, B*, 2009, **143**, 302.
5 K. Akamatsu, S. Ikeda, H. Nawafune and S. Deki, *Chem. Mater.*, 2003, **15**, 2488.
6 S. Ikeda, K. Akamatsu, H. Nawafune, T. Nishino and S. Deki, *J. Phys. Chem.*, B, 2004, **108**, 15599.
7 Z. Wu, D. Wu, S. Qi, T. Zhang and R. Jin, *Thin Solid Films*, 2005, **493**, 179.
8 Z. Wu, D. Wu, W. Yang and R. Jin, *J. Mater. Chem.*, 2006, **16**, 310.
9 T. Yang, Y. Z. Yu, L. S. Zhu, X. Wu, X. H. Wang and J. Zhang, *Sens. Actuators, B*, 2015, **208**, 327.
10 D. Kim, G. Shin, Y. J. Kang, W. Kim and J. S. Ha, *Acs Nano*, 2013, **7**, 7975.
11 S. Y. Hong, J. Yoon, S. W. Jin, Y. Lim, S.-J. Lee, G. Zi and J. S. Ha, *Acs Nano*, 2014, **8**, 8844.
12 P. Yang and W. Mai, *Nano Energy*, 2014, **8**, 274.
13 G. Xiong, C. Meng, R. G. Reifenberger, P. P. Irazoqui and T. S. Fisher, *Electroanal.*, 2014, **26**, 30.
14 J. Chmiola, C. Largeot, P. L. Taberna, P. Simon and Y. Gogotsi, *Science*, 2010, **328**, 480.
15 M. Beidaghi and C. Wang, *Adv. Funct. Mater.*, 2012, **22**, 4501.
16 T. M. Dinh, K. Armstrong, D. Guay and D. Pech, *J. Phys. Chem.*, A 2014, **2**, 7170.
17 J. Lin, C. Zhang, Z. Yan, Y. Zhu, Z. Peng, R. H. Hauge, D. Natelson and J. M. Tour, *Nano Lett.*, 2013, **13**, 72.
18 D. Pech, M. Brunet, H. Durou, P. Huang, V. Mochalin, Y. Gogotsi, P.-L. Taberna and P. Simon, *Nat. Nanotechnol.*, 2010, **5**, 651
19 W. Si, C. Yan, Y. Chen, S. Oswald, L. Han and O. G. Schmidt, *Energy Environ. Sci.*, 2013, **6**, 3218.
20 Z. S. Wu, K. Parvez, X. L. Feng and K. Mullen, *Nat. Commun.*, 2013, **4**, 2487.
21 Z. S. Wu, K. Parvez, A. Winter, H. Vieker, X. Liu, S. Han, A. Turchanin, X. Feng and K. Muellen, *Adv. Mater.*, 2014, **26**, 4552.
22 M. F. El-Kady and R. B. Kaner, *Nat. Commun.*, 2013, **4**, 1475.
23 Y. Wang, Y. Shi, C. X. Zhao, J. I. Wong, X. W. Sun and H. Y. Yang, *Nanotechnology*, 2014, **25**, 094010.
24 K. Mun Sek, B. Hsia, C. Carraro and R. Maboudian, *Carbon*, 2014, **74**, 163.
25 W. Gao, N. Singh, L. Song, Z. Liu, A. L. M. Reddy, L. Ci, R. Vajtai, Q. Zhang, B. Wei and P. M. Ajayan, *Nat. Nanotechnol.*, 2011, **6**, 496.
26 S. Wang, B. Hsia, C. Carraro and R. Maboudian, *J. Phys. Chem. A*, 2014, **2**, 7997.
27 L. Cao, S. Yang, W. Gao, Z. Liu, Y. Gong, L. Ma, G. Shi, S. Lei, Y. Zhang, S. Zhang, R. Vajtai and P. M. Ajayan, *Small*, 2013, **9**, 2905.
28 H. Hu, K. Zhang, S. Li, S. Ji and C. Ye, *J. Phys. Chem. A*, 2014, **2**, 20916.
29 C.-C. Liu, D.-S. Tsai, W.-H. Chung, K.-W. Li, K.-Y. Lee and Y.-S. Huang, *J. Power Sources*, 2011, **196**, 5761.
30 Z. Q. Niu, L. Zhang, L. Liu, B. W. Zhu, H. B. Dong and X. D. Chen, *Adv. Mater.*, 2013, **25**, 4035.
31 S. Liu, J. Xie, H. Li, Y. Wang, H. Y. Yang, T. Zhu, S. Zhang, G. Cao and X. Zhao, *J. Phys. Chem. A*, 2014, **2**, 18125.
32 M. Beidaghi, W. Chen and C. L. Wang, *J. Power Sources*, 2011, **196**, 2403.
33 V. Strong, S. Dubin, M. F. El-Kady, A. Lech, Y. Wang, B. H. Weiller and R. B. Kaner, *ACS Nano*, 2012, **6**, 1395.
34 M. F. El-Kady, V. Strong, S. Dubin and R. B. Kaner, *Science*, 2012, **335**, 1326.
35 F. Wen, C. Hao, J. Xiang, L. Wang, H. Hou, Z. Su, W. Hu and Z. Liu, *Carbon* 2014, **75**, 236.
36 B. Hsia, J. Marschewski, S. Wang, J. B. In, C. Carraro, D. Poulikakos, C. P. Grigoropoulos and R. Maboudian, *Nanotechnology*, 2014, **25**, 055401.
37 K. Wang, W. Zou, B. Quan, A. Yu, H. Wu, P. Jiang and Z. Wei, Adv. *Energy Mater.*, 2011, **1**, 1068.
38 L. L. Peng, X. Peng, B. R. Liu, C. Z. Wu, Y. Xie and G. H. Yu, *Nano Lett.*, 2013, **13**, 2151.
39 S. Liu, J. Xie, H. Li, Y. Wang, H. Y. Yang, T. Zhu, S. Zhang, G. Cao and X. Zhao, *J. Phys. Chem.*, A 2014, **2**, 18125.

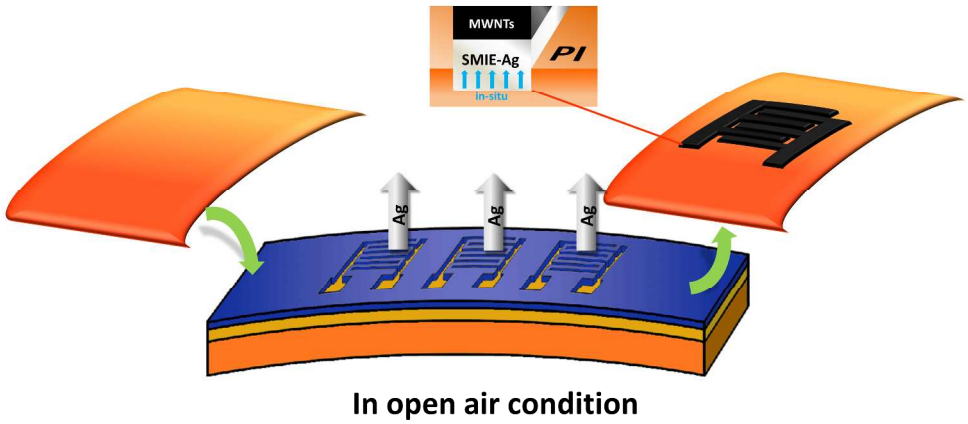

The flexible MSCs with SMIE technique is completed in open air and does not involve any complicated clean room processes. MSCs of this work offers high power density, high flexibility and long endurance, especially the ultra-high mechanical strength.